Iranian Journal of Science and Technology, Transactions of Mechanical Engineering (2021) 45:863–878
https://doi.org/10.1007/s40997-019-00337-5

RESEARCH PAPER

Transverse Vibration of Thin Rectangular Orthotropic Plates on Translational and Rotational Elastic Edge Supports: A Semi-analytical Approach

R. K. Praharaj[1] · N. Datta[1] · M. R. Sunny[1] · Y. Verma[1]

Received: 8 March 2019 / Accepted: 26 November 2019 / Published online: 5 December 2019

Abstract
The free vibration analysis of thin orthotropic plates with elastically constrained edges is presented using the energy-based Rayleigh–Ritz (RR) method. Various edge conditions are modeled with rotational and translational linear springs. The complete set of admissible functions, which is a combination of (1) trigonometric functions, (2) the unit function, (3) the linear function, and (4) the lowest order polynomial, has been used in the RR method. It has been demonstrated that the use of a combination of the lowest order polynomial and the cosine series results in a rapid convergence of the solution, without any ill-conditioning of the admissible functions upon expansion. In particular, this work proposes a simple guideline for determining a set of trial functions that can be universally utilized for the vibration analysis of plates with non-classical boundary conditions. The convergence and exactness of this approach have been demonstrated through several examples. The results indicate that the elastically restrained stiffness and the plate aspect ratio impact the frequency parameters considerably.

Keywords Orthotropic plate · Non-classical edge · Trial function · Rayleigh–Ritz method · Convergence

List of Symbols

x, y, z	Axis of the reference system
a	Length of the plate (m)
b	Breadth of the plate (m)
h	Thickness of the plate (m)
A	Cross-sectional area (m^2)
E_1	Young's modulus of the material in bending for the x direction (N/m^2)
E_2	Young's modulus of the material in bending for the y direction (N/m^2)
G_{12}	Shear modulus of the material in bending in xy plane (N/m^2)
D_{ij}	Standard bending rigidities
υ_{12}	Major Poisson's ratio (–)
υ_{21}	Minor Poisson's ratio (–)
ρ	Mass density of the specified material (kg/m^3)
ω	Dimensional plate natural frequency (rad/s)
Ω	Non-dimensional plate natural circular frequency (–)
M_x, M_y	Bending moments
Q_x, Q_x	Shear forces
M_{xy}	Twisting moments
$\boldsymbol{K}$	Stiffness matrix
$\boldsymbol{M}$	Mass matrix
A_{ij}	Weight coefficients
T	Kinetic energy of the plate (J)
U	Strain energy of the plate (J)
K_{T}	Non-dimensional translational spring constant (–)
K_{R}	Non-dimensional rotational spring constant (–)
α	Aspect ratio (–)
$W(x, y)$	Transverse displacement of the plate (m)

1 Introduction

Orthotropic plates, due to their high strength-to-weight ratio, have wide applications in various structural engineering fields like civil constructions, aerospace structures, and marine constructions. The extensive use of orthotropic plates requires the precise vibration characteristics for long-lasting engineering design. In the industry, the finite element method-based softwares are used for vibration analysis, leading to the natural frequencies, mode shapes, and dynamic responses of the structure. However, the non-classical boundary conditions

✉ R. K. Praharaj
rajendra.praharaj@gmail.com

[1] Indian Institute of Technology, Kharagpur, India

may be often difficult to model. Also, repeatedly changing the non-classical boundary conditions during the design iterations becomes a long-drawn out process in the commercial software. Therefore, during the initial design stage, when the boundary conditions (along with the geometric and material properties) are yet to be finalized, it is useful to have a reliable and fast analytical/semi-analytical methodology to benchmark the vibration parameters of the structure.

The free vibration of orthotropic plates with classical boundary conditions has been extensively studied in recent decades. Hearmon (1959) studied the free vibration of orthotropic plates considering beam functions as the trial functions in the *Rayleigh–Ritz method*. The beam functions were expressed as linear combinations of trigonometric and hyperbolic functions, with unknown coefficients which are to be determined for each set of boundary conditions by solving a system of four coupled ordinary differential equations. This makes the use of beam functions a very tedious process. In addition, a set of trial functions using hyperbolic and trigonometric functions are prone to numerical instability when more terms are incorporated in the solution. The *Rayleigh–Ritz method* is one of the suitable and convenient methods to calculate the eigenvalues of rectangular orthotropic plates due to its conceptual simplicity (Meirovitch 1975). Dickinson and Di Blasio (1986) used orthogonal polynomials as admissible functions in the *Rayleigh–Ritz method* to study the transverse vibration and buckling of orthotropic and isotropic rectangular plates for classical boundary conditions. Bapat et al. (1988) investigated the effects of the elastic edge support stiffness and its distribution on the natural frequencies, shear force, and bending moment of the thin plate. Gorman (1982) applied the *superposition method* to study free vibration of the isotropic plate and then extended it for the application to completely free orthotropic plates (Gorman 1993), clamped orthotropic plates (Gorman 1990), and point-supported orthotropic plates (Gorman 1994). Dalaei and Kerr (1996) investigated the free vibration of thin rectangular orthotropic plates with fully fixed edges using the extended *Kantorovich method*. Rossi et al. (1998) studied the vibration of orthotropic plates with free edges using an optimized *Rayleigh–Ritz method*. The results were compared with those calculated using the finite element method. Hurlebaus et al. (2001) studied the modal characteristics of a completely free orthotropic thin plate by an exact solution method. Ahmadian and Zangeneh (2002) applied efficient superelements to study the fundamental frequencies of isotropic and orthotropic plates with various classical boundaries. Li (2004) studied the vibration of isotropic plates with elastic edge supports using *Rayleigh–Ritz method*. The displacement functions are a combination of cosine Fourier series and fourth-order Legendre polynomial. The coefficients of the Legendre polynomial functions are required to be calculated for every boundary

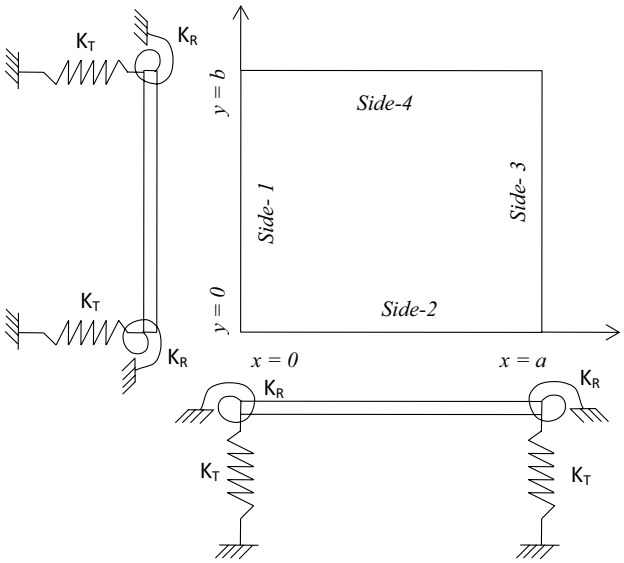

Fig. 1 Rectangular plate elastically restrained along edges

condition. In addition, it was reported that the use of polynomials in higher-order analysis led to numerically unstable solutions due to round-off errors. Biancolini et al. (2005) studied the free vibration of thin orthotropic rectangular plates with classical edges by an approximate solution technique and validated them with the finite element method.

Li and Cheng (2005) studied the nonlinear vibration of orthotropic plates using the *differential quadrature method* (DQM). Huang et al. (2005) investigated the free vibration of orthotropic rectangular plates with variable thickness in one or two directions, using a discrete method, for only the classical boundary conditions. Xing and Liu (2009) presented an exact solution technique for the free vibration of thin orthotropic plates having combinations of simply supported and clamped conditions only. Hsu (2010) investigated the vibration of a thin plate resting on an elastic foundation using the *Rayleigh–Ritz method*. Jafari and Eftekhari (2011) calculated the non-dimensional frequency parameters and critical bucking loads of thin orthotropic plates for classical boundary conditions, using the efficient mixed *Ritz-differential quadrature method*. Shi et al. (2014) investigated the free vibration of thin orthotropic plate with arbitrary elastic supports using the *Spectro-Geometric Method*. Xing and Xu (2013) investigated the free vibration of rectangular thin plates with at least two adjacent clamped edges and others as arbitrary combinations of the simply supported, guided, and clamped type. Datta and Verma (2018) studied the influence of the rigid-body modes on the vibration modes of thin plates. Verma and Datta (2018) investigated the free vibration of the Kirchhoff's plate having edges supported only by variable translational springs, by using the *Rayleigh–Ritz method*. Zhang et al. (2019) recently investigated the free transverse vibration of the rotationally restrained rectangular orthotropic plates using the method of finite integral transform.

The past investigations on orthotropic plates are mostly limited to classical boundary conditions and their possible combinations. However, the realistic non-classical boundary conditions are often encountered in practical engineering applications, where the edge supports can be modeled as uniformly distributed translational and/or rotational springs. This work presents a new complete set of orthogonal admissible functions, satisfying all the beam boundary conditions, as well as the rigid-body mode shapes for free–free and sliding–sliding beams. Only four simple functions are shown to be sufficient to together act as admissible functions, proving to be versatile for the vibration analysis of thin orthotropic/isotropic plates with any classical/non-classical boundary conditions, for any aspect ratio. This greatly reduces the tedious process of choosing the correct admissible functions of individual classical boundary conditions and the exponentially cumbersome process of choosing the admissible functions for non-classical boundary conditions. The availability of admissible functions bypasses the cumbersome numerical analyses for non-classical boundary conditions, giving the results with speed and accuracy.

2 Orthotropic Rectangular Plate Vibration

A thin, orthotropic, homogenous, rectangular plate is shown in Fig. 1. The edge constraints are non-classical, and thus, they are modeled as translational and rotational springs distributed uniformly over the edges. The stiffness distribution for both translational and rotational springs can be specified independently with respect to the flexural rigidity of the plate, such that they can represent non-classical boundary conditions (of practical interest) and all classical boundary conditions (when spring stiffness equals either infinity or zero). The free edge (*F*) refers to a special case of elastic support when the stiffness values of both rotational and translational springs are set to zero. Similarly, for the clamped edge (*C*), stiffness values for both the springs are set to infinity (represented by 10^8 in the analysis). The simple supported (*S*) case can be represented by setting an infinite stiffness for the translational spring and a zero stiffness for the rotational spring. The opposite is done for the sliding case (*G*).

The governing differential equation of free transverse vibration of a thin orthotropic rectangular plate is given as Hsu (2010) follows:

$$D_{11}\frac{\partial^4 Z(x,y,t)}{\partial x^4} + 2\left(D_{12}+2D_{66}\right)\frac{\partial^4 Z(x,y,t)}{\partial x^2\partial y^2} + D_{22}\frac{\partial^4 Z(x,y,t)}{\partial y^4} + \rho h\frac{\partial^2 Z(x,y,t)}{\partial t^2} = 0 \tag{1}$$

The transverse displacement can be expressed as:

$$Z(x,y,t) = W(x,y)\mathrm{e}^{i\omega t} \tag{2}$$

Substituting Eq. (2) in Eq. (1), the spatial component of Eq. (1) can be rewritten as

$$D_{11}\frac{\partial^4 W(x,y)}{\partial x^4} + 2\left(D_{12}+2D_{66}\right)\frac{\partial^4 W(x,y)}{\partial x^2\partial y^2} + D_{22}\frac{\partial^4 W(x,y)}{\partial y^4} = \rho h\omega^2 W(x,y) \tag{3}$$

where $W(x,y)$ is the space-wise flexural displacement, D_{ij} are the flexural rigidities, ρ is the density of the plate material, h is the plate thickness, and ω is the circular frequency of vibration. For an orthotropic plate, the bending stiffness coefficients are given by:

$$D_{ij} = \int_{-\frac{h}{2}}^{\frac{h}{2}} P_{ij}z^2\mathrm{d}z \quad \text{for } i,j = 1,2,6 \tag{4}$$

$$\text{where } P_{11} = \frac{E_1}{1-\upsilon_{12}\upsilon_{21}}, P_{12} = \frac{E_2\upsilon_{12}}{1-\upsilon_{12}\upsilon_{21}}, P_{21} = \frac{E_1\upsilon_{21}}{1-\upsilon_{12}\upsilon_{21}}, P_{22} = \frac{E_2}{1-\upsilon_{12}\upsilon_{21}} \text{ and } D_{66} = G_{12}\frac{h^3}{12} \tag{5–9}$$

where E_1 and E_2 are Young's modulus of the material in 1 and 2 directions, respectively, υ_{12} is the Poisson's ratio for transverse strain in the second direction due to applied stress in the first direction, υ_{21} is the Poisson's ratio for transverse strain in the first direction due to applied stress in the second direction, and G_{12} is the shear modulus in the 1–2 plane. For orthotropic materials, the elastic properties have two perpendicular planes of symmetry, and thus, they are characterized by four independent elastic constants E_1, E_2, G_{12}, and ν_{12}, with $E_2\nu_{12} = E_1\nu_{21}$.

The bending moment, the twisting moment, and the shear force are, respectively, expressed in terms of the transverse displacement as follows:

$$M_x = -D_{11}\frac{\partial^2 W(x,y)}{\partial x^2} - D_{12}\frac{\partial^2 W(x,y)}{\partial y^2}; \quad M_y = -D_{22}\frac{\partial^2 W(x,y)}{\partial y^2} - D_{12}\frac{\partial^2 W(x,y)}{\partial x^2} \tag{10–11}$$

$$M_{xy} = -2D_{66}\frac{\partial^2 W(x,y)}{\partial x\partial y} \tag{12}$$

$$Q_x = -D_{11}\frac{\partial^3 W(x,y)}{\partial x^3} - \left(D_{12}+4D_{66}\right)\frac{\partial^3 W(x,y)}{\partial x\partial y^2} \tag{13}$$

$$Q_y = -D_{22}\frac{\partial^3 W(x,y)}{\partial y^3} - \left(D_{12}+4D_{66}\right)\frac{\partial^3 W(x,y)}{\partial x^2\partial y} \tag{14}$$

Here, the edge is elastically constrained with translational and rotational springs. Thus, the shear force developed at the edges is balanced by the translational spring force generated due to the deflection. Similarly, the bending moment at the edges is balanced by the moment generated by rotational spring due to the slope. The boundary conditions for an elastically restrained plate are expressed as:

$$k_{Tx0}W(x,y) = Q_x = -D_{11}\frac{\partial^3 W(x,y)}{\partial x^3} - \left(D_{12}+4D_{66}\right)\frac{\partial^3 W(x,y)}{\partial x \partial y^2} \text{ at } x=0 \tag{15}$$

$$k_{Rx0}\frac{\partial W(x,y)}{\partial x} = -M_x = D_{11}\frac{\partial^2 W(x,y)}{\partial x^2} + D_{12}\frac{\partial^2 W(x,y)}{\partial y^2} \text{ at } x=0 \tag{16}$$

$$k_{Tx1}W(x,y) = -Q_x = D_{11}\frac{\partial^3 W(x,y)}{\partial x^3} + \left(D_{12}+4D_{66}\right)\frac{\partial^3 W(x,y)}{\partial x \partial y^2} \text{ at } x=a \tag{17}$$

$$k_{Rx1}\frac{\partial W(x,y)}{\partial x} = M_x = -D_{11}\frac{\partial^2 W(x,y)}{\partial x^2} - D_{12}\frac{\partial^2 W(x,y)}{\partial y^2} \text{ at } x=a \tag{18}$$

$$k_{Ty0}W(x,y) = Q_y = -D_{22}\frac{\partial^3 W(x,y)}{\partial y^3} - \left(D_{12}+4D_{66}\right)\frac{\partial^3 W(x,y)}{\partial x^2 \partial y} \text{ at } y=0 \tag{19}$$

$$k_{Ry0}\frac{\partial W(x,y)}{\partial y} = -M_y = D_{22}\frac{\partial^2 W(x,y)}{\partial y^2} + D_{12}\frac{\partial^2 W(x,y)}{\partial x^2} \text{ at } y=0 \tag{20}$$

$$k_{Ty1}W(x,y) = -Q_y = D_{22}\frac{\partial^3 W(x,y)}{\partial y^3} + \left(D_{12}+4D_{66}\right)\frac{\partial^3 W(x,y)}{\partial x^2 \partial y} \text{ at } y=b \tag{21}$$

$$k_{Ry1}\frac{\partial W(x,y)}{\partial y} = M_y = -D_{22}\frac{\partial^2 W(x,y)}{\partial y^2} - D_{12}\frac{\partial^2 W(x,y)}{\partial x^2} \text{ at } y=b \tag{22}$$

where k_{Tx0} and k_{Tx1} (k_{Ty0} and k_{Ty1}) are the translational spring stiffness per unit length and k_{Rx0} and k_{Rx1} (k_{Ry0} and k_{Ry1}) are the rotational spring stiffness per unit length, located along edges of the plate at ($x=0, x=a, y=0$ and $y=b$), respectively. Classical boundary conditions can be obtained by setting appropriate extreme values to the spring constants. Generally, an exact analytical solution for plates with non-classical [Eq. (15–22)] is not possible. Therefore, to obtain the approximate solutions, the energy-based Rayleigh–Ritz method (RRM) has been used with the complete set of admissible functions, efficiently converging to the exact solution.

The strain potential energy (U) of orthotropic Kirchhoff's plates with elastically restrained against translational and rotational edges is given as

$$\begin{aligned} U = {} & \frac{1}{2}\int_0^a\int_0^b \left(D_{11}\left(\frac{\partial^2 W(x,y)}{\partial x^2}\right)^2 + 2D_{12}\frac{\partial^2 W(x,y)}{\partial x^2}\frac{\partial^2 W(x,y)}{\partial y^2} \right. \\ & \left. +4D_{66}\left(\frac{\partial^2 W(x,y)}{\partial x \partial y}\right)^2 + D_{22}\left(\frac{\partial^2 W(x,y)}{\partial y^2}\right)^2 \right) \mathrm{d}x\mathrm{d}y \\ & + \frac{1}{2}\int_0^a k_{Ry0}\left(\frac{\partial W(x,0)}{\partial y}\right)^2 \mathrm{d}x + \frac{1}{2}\int_0^a k_{Ry1}\left(\frac{\partial W(x,b)}{\partial y}\right)^2 \mathrm{d}x \\ & + \frac{1}{2}\int_0^b k_{Rx0}\left(\frac{\partial W(0,y)}{\partial x}\right)^2 \mathrm{d}y + \frac{1}{2}\int_0^b k_{Rx1}\left(\frac{\partial W(a,y)}{\partial y}\right)^2 \mathrm{d}y \\ & + \frac{1}{2}\int_0^a k_{Ty0}(W(x,0))^2 \mathrm{d}x + \frac{1}{2}\int_0^a k_{Ty1}(W(x,b))^2 \mathrm{d}x \\ & + \frac{1}{2}\int_0^b k_{Tx0}(W(0,y))^2 \mathrm{d}y + \frac{1}{2}\int_0^b k_{Tx1}(W(a,y))^2 \mathrm{d}y \end{aligned} \tag{23}$$

The kinetic energy (T) of the orthotropic plate is given as

$$T = \frac{1}{2}\rho h\omega^2 \int_0^a\int_0^b (W(x,y))^2 \mathrm{d}x\mathrm{d}y \tag{24}$$

The amplitude of the transverse deflection of the plate is expressed as the weighted superposition of the admissible functions in either direction as:

$$W(x,y) = \sum_{i=1}^{\text{modex}}\sum_{j=1}^{\text{modey}} A_{ij}\emptyset_i(x)\emptyset_j(y) \tag{25}$$

where 'modex' and 'modey' are the number of trial functions considered in x direction and y direction, respectively, and A_{ij} are the unknown coefficients. $\emptyset_j(x)$ and $\emptyset_j(y)$ are the set of admissible beam functions in x and y directions, respectively. To investigate a wide range of aspect ratio, it is required to non-dimensionalize the system of equations with the non-dimensional spatial coordinates of the plate $\xi = \frac{x}{b}$, $\eta = \frac{y}{b}$ and aspect ratio $(\alpha) = \frac{a}{b}$. Thus, the above strain energy (Eq. 23) and kinetic energy (Eq. 24) expressions can be rewritten as:

$$
\begin{aligned}
U_{\text{Plate}} = {} & \frac{D_{11}}{2}\frac{b}{a^3}\int_0^1\int_0^1\left[\left(\frac{\partial^2 W}{\partial\xi^2}\right)^2 + 2\frac{D_{12}}{D_{11}}\frac{a^2}{b^2}\frac{\partial^2 W}{\partial\xi^2}\frac{\partial^2 W}{\partial\eta^2} + 4\frac{D_{66}}{D_{11}}\frac{a^2}{b^2}\left(\frac{\partial^2 W}{\partial\xi\partial\eta}\right)^2 + \frac{D_{22}}{D_{11}}\frac{a^4}{b^4}\frac{\partial^4 W}{\partial\eta^4}\right]\partial\xi\partial\eta \\
& + \frac{1}{2}\int_0^1 k_{\text{Rx0}}\frac{b}{a^2}\left(\frac{\partial W(0,\eta)}{\partial\xi}\right)^2 \mathrm{d}\eta + \frac{1}{2}\int_0^1 k_{\text{Rx1}}\frac{b}{a^2}\left(\frac{\partial W(1,\eta)}{\partial\xi}\right)^2 \mathrm{d}\eta + \frac{1}{2}\int_0^1 k_{\text{Ry0}}\frac{a}{b^2}\left(\frac{\partial W(\xi,0)}{\partial\eta}\right)^2 \mathrm{d}\xi \\
& + \frac{1}{2}\int_0^1 k_{\text{Ry1}}\frac{a}{b^2}\left(\frac{\partial W(\xi,1)}{\partial\eta}\right)^2 \mathrm{d}\xi + \frac{1}{2}\int_0^1 k_{\text{Ty0}}a(W(\xi,0))^2\mathrm{d}\xi + \frac{1}{2}\int_0^1 k_{\text{Ty1}}a(W(\xi,1))^2\mathrm{d}\xi \\
& + \frac{1}{2}\int_0^1 k_{\text{Tx0}}b(W(0,\eta))^2\mathrm{d}\eta + \frac{1}{2}\int_0^1 k_{\text{Tx1}}b(W(1,\eta))^2\mathrm{d}\eta
\end{aligned} \tag{26}
$$

$$
T_{\text{Plate}} = \frac{1}{2}\rho h\omega^2 ab\int_0^1\int_0^1 W(\xi,\eta)^2\mathrm{d}\xi\mathrm{d}\eta \tag{27}
$$

The RRM is used to minimize the energy functional (i.e., the difference of total strain energy and total kinetic energy) with respect to unknown coefficients, which leads to a set of linear homogeneous equations:

$$
\left(\frac{\partial}{\partial A_{ij}}\right)\left[U_{\text{Plate}} - T_{\text{Plate}}\right] = 0 \tag{28}
$$

This generates a non-dimensional eigenvalue problem:

$$
\left([\boldsymbol{K}] - \Omega^2[\boldsymbol{M}]\right)\{\boldsymbol{A}\} = 0 \tag{29}
$$

$$
\boldsymbol{M}_{ijkp} = A_{i,k}^{(0,0)}B_{j,p}^{(0,0)} \tag{31}
$$

where $K_{\text{R1}} = \dfrac{k_{\text{Rx0}}a}{D_{11}}, K_{\text{R2}} = \dfrac{k_{Ey0}b}{D_{11}}, K_{\text{R3}} = \dfrac{k_{\text{Rx1}}a}{D_{11}},$

$K_{\text{R4}} = \dfrac{k_{\text{Ry1}b}}{D_{11}}, K_{\text{T1}} = \dfrac{k_{\text{Tx0}}a^3}{D_{11}}, K_{T2} = \dfrac{k_{\text{Ty0}}b^3}{D_{11}},$

$K_{\text{T3}} = \dfrac{k_{\text{Tx1}}a^3}{D_{11}}, K_{\text{T4}} = \dfrac{k_{\text{Ty1}}b^3}{D_{11}};$

$$
A_{i.k}^{m,n} = \int_0^1 \frac{\mathrm{d}^m\phi_i(\xi)}{\mathrm{d}\xi^m}\frac{\mathrm{d}^m\phi_k(\xi)}{\mathrm{d}\xi^n}\mathrm{d}\xi;
$$

$$
B_{j,p}^{m,n} = \int_0^1 \frac{\mathrm{d}^m\phi_j(\eta)}{\mathrm{d}\eta^m}\frac{\mathrm{d}^n\phi_p(\eta)}{\mathrm{d}\eta^n}\mathrm{d}\eta
$$

$$
\begin{aligned}
K_{ijkp} = {} & A_{ik}^{(2,2)}B_{jp}^{(0,0)} + 2\frac{D_{12}}{D_{11}}\alpha^2\left[A_{ik}^{(0,2)}B_{jp}^{(2,0)} + A_{ik}^{(2,0)}B_{jp}^{(0,2)}\right] + 4\frac{D_{66}}{D_{11}}\alpha^2 A_{ik}^{(1,1)}B_{jp}^{(1,1)} + \frac{D_{22}}{D_{11}}\alpha^4 A_{ik}^{(0,0)}B_{jp}^{(2,2)} \\
& + K_{\text{R1}}\frac{\partial\emptyset_i(0)}{\partial\xi}\frac{\partial\emptyset_k(0)}{\partial\xi}B_{jp}^{(0,0)} + K_{\text{R3}}\frac{\partial\emptyset_i(1)}{\partial\xi}\frac{\partial\emptyset_k(1)}{\partial\xi}B_{jp}^{(0,0)} + \alpha^4 K_{R4}\frac{\partial\emptyset_i(0)}{\partial\eta}\frac{\partial\emptyset_k(0)}{\partial\eta}A_{ik}^{(0,0)} \\
& + \alpha^4 K_{\text{R2}}\frac{\partial\emptyset_i(1)}{\partial\eta}\frac{\partial\emptyset_k(1)}{\partial\eta}A_{ik}^{(0,0)} + K_{\text{T1}}\phi_i(0)\phi_k(0)B_{jp}^{(0,0)} + K_{\text{T3}}\phi_i(1)\phi_k(1)B_{jp}^{(0,0)} \\
& + \alpha^4 K_{\text{T4}}\phi_j(0)\phi_p(0)A_{ik}^{(0,0)} + \alpha^4 K_{\text{T2}}\phi_j(1)\phi_p(1)A_{ik}^{(0,0)}
\end{aligned} \tag{30}
$$

where $m, n = 0, 1, 2$ and $i, k, j, p = 1, 2, 3 \ldots, n$. $[\boldsymbol{K}]$ and $[\boldsymbol{M}]$ are the non-dimensional stiffness matrix and mass matrix, respectively; $\{\boldsymbol{A}\}$ denotes the unknown coefficients in the series expansion. Here, $\Omega^2 = \frac{\rho h \omega^2 a^2 b^2}{D_{11}}$ stands for the non-dimensional frequency parameter, where ω^2 is the dimensional frequency parameter (rad/s). The natural frequencies and corresponding eigenvectors are determined by solving Eq. (29). The mode shapes can be found by using Eq. (25).

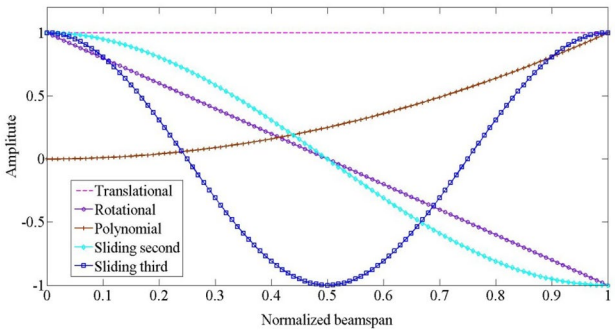

Fig. 2 First five admissible functions

3 Building a Set of Admissible Functions

Several researchers have specified the guidelines to select a set of admissible functions for plate vibration analysis, e.g., Oosterhout et al. (1995) as follows:

(a) The set of admissible functions must satisfy the geometric boundary conditions.
(b) The admissible functions must be linearly independent of each other.
(c) The second-order derivatives of the admissible functions must exist (required to capture flexural modes).
(d) The set of admissible functions should be able to represent all the modes of vibration.

Based on the above guidelines, this work presents a complete set of admissible functions to model an unconstrained (FFFF) plate, whose RRM analysis converges fast without numerical instabilities. The complex boundary conditions can be modeled by adding appropriate translational and rotational spring stiffness at the edges. The set of admissible functions should include the translational and rotational rigid-body modes of the beam and should also satisfy the essential boundary conditions as a complete series of functions, rather than each individual function. The rigid-body modes of the beam have been included in the set of admissible functions by a unit term and a linear function. The unit term represents the translational rigid mode or the heave mode of the beam, and the linear function represents the rotational rigid mode or the pitch mode. To keep the solution free from numerical instabilities, the minimum number of possible lowest order polynomial functions is to be included in the complete set of admissible functions. Next, to satisfy all the geometrical boundary conditions, it is necessary to include an additional term which satisfies a second nonzero slope at the end of the beam; thus, the lowest order polynomial has been added to the series. Monterrubio and Ilanko (2015) stated that for most of the boundary conditions, the convergence rates are faster with cosine series as compared to the sine series. Actually, the cosine series show their rapid rate of convergence for sliding-type boundary condition, while the sine series is suitable for the simply supported conditions. Cosine functions satisfy the orthogonality properties which makes the mass and stiffness matrix sparser or diagonally dominant, leading to higher computational efficiency and faster convergence of

Table 1 Material properties of the orthotropic plate

	Material	E_1 (GPa)	E_2 (GPa)	G_{12} (GPa)	ν_{12}	ρ (kg/m^3)
M1	B-boron/epoxy	208	18.9	5.7	0.23	2000
M2	T-graphite/epoxy	185	10.5	7.3	0.28	1600

Table 2 Convergence study of frequency parameter $\Omega = \sqrt[4]{\omega^2 \rho h a^2 b^2 / D_{11}}$ square F–F–F–F orthotropic plates M1

No of terms	Mode sequence									
	1	2	3	4	5	6	7	8	9	10
5	1.959	2.585	3.212	4.724	4.771	5.055	5.302	5.324	6.617	7.191
10	1.953	2.585	3.207	4.287	4.675	4.723	4.869	5.316	6.032	6.160
15	1.953	2.585	3.207	4.287	4.675	4.723	4.869	5.315	6.032	6.159
20	1.953	2.585	3.207	4.287	4.674	4.723	4.869	5.315	6.032	6.158
Ref [a^*]	1.960	2.590	3.220	4.310	4.680	4.730	4.870	5.310	6.040	6.140

a^*: Shi et al. (2014)

Table 3 Convergence study of the fundamental frequency of square CCCC isotropic and orthotropic plates M1

	CCCC isotropic plate $\left[\Omega = \sqrt[2]{\omega^2 \rho h a^2 b^2 / D}\right]$			CCCC orthotropic plate $\left[\Omega = \sqrt[4]{\omega^2 \rho h a^2 b^2 / D}\right]$		
# Terms	Result	Exact	% Error	Result	Exact	% Error
5	37.221	35.985	3.433	4.9488	4.880	1.390
6	37.220	35.985	3.433	4.9484	4.880	1.382
7	36.295	35.985	0.861	4.9079	4.880	0.568
8	36.295	35.985	0.861	4.9073	4.880	0.556
9	36.105	35.985	0.335	4.8992	4.880	0.393
10	36.105	35.985	0.334	4.8985	4.880	0.378
11	36.043	35.985	0.162	4.8959	4.880	0.324
12	36.043	35.985	0.162	4.8951	4.880	0.308
13	36.017	35.985	0.090	4.8939	4.880	0.285
14	36.017	35.985	0.090	4.8931	4.880	0.268
15	36.005	35.985	0.055	4.8925	4.880	0.255
16	36.005	35.985	0.055	4.8916	4.880	0.238
17	35.998	35.985	0.035	4.8913	4.880	0.230
18	35.998	35.985	0.035	4.8904	4.880	0.212
19	35.993	35.985	0.023	4.8901	4.880	0.207
20	35.993	35.985	0.023	4.8892	4.880	0.188
21	35.993	35.985	0.023	4.8890	4.880	0.184
22	35.991	35.985	0.016	4.8881	4.880	0.165
23	35.989	35.985	0.011	4.8879	4.880	0.162
24	35.989	35.985	0.011	4.8869	4.880	0.142
25	35.988	35.985	0.007	4.8868	4.880	0.139
26	35.987	35.985	0.007	4.8858	4.880	0.119
27	35.987	35.985	0.005	4.8857	4.880	0.116
28	35.987	35.985	0.004	4.8847	4.880	0.096
29	35.986	35.985	0.002	4.8845	4.880	0.093
30	35.986	35.985	0.002	4.8835	4.880	0.072
31				4.8834	4.880	0.069
32				4.8823	4.880	0.047
33				4.8822	4.880	0.044
34				4.8811	4.880	0.022
35				4.8809	4.880	0.019
36				4.8808	4.880	0.016
37				4.8805	4.880	0.011
38				4.8805	4.880	0.009
39				4.8803	4.880	0.006
40				4.8803	4.880	0.006

the solution. Therefore, the cosine series has been selected to complete the set of admissible functions. The selection of proper admissible functions has a major role in the present energy-based method because the exactness of the solution is largely influenced by them. The final set of admissible functions are:

$$\phi_1(x) = 1; \phi_2(x) = \left(1 - \frac{2x}{L}\right);$$
$$\phi_3(x) = \left(\frac{x}{L}\right)^2; \phi_i(x) = \cos\frac{(i-1)\pi x}{L}, \quad \text{for } i = 4, 5 \ldots, n \tag{32(a–d))}$$

The admissible functions $\emptyset_i(x)$ used in the present study are given in Eq. (32), and the first five admissible functions are shown in Fig. 2. It clearly indicates that the admissible functions selected for the present study permit nonzero displacement and translation at both ends of the beam. The complete set of admissible functions satisfies the geometric boundary conditions at both ends of the free–free beam. In this study, the set of admissible functions is the same for both x and y directions.

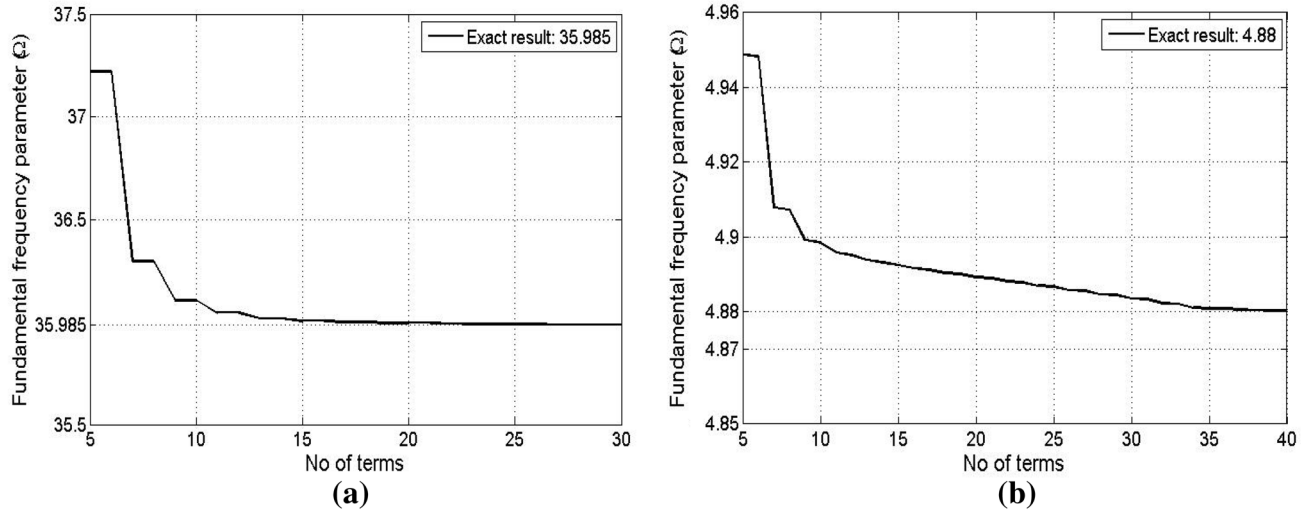

Fig. 3 Convergence study: **a** isotropic square plate and **b** orthotropic square plate M1

Table 4 Non-dimensional frequency parameter $\Omega = \sqrt[4]{\omega^2 \rho h a^2 b^2 / D_{11}}$ for rectangular F–F–F–F orthotropic plates M1

a/*b*	Method	Mode sequence									
		1	2	3	4	5	6	7	8	9	10
0.33	Present	0.86	1.10	1.43	1.61	2.00	2.08	2.54	2.58	3.03	3.15
	Ref [*a**]	0.86	1.11	1.14	1.62	2.01	2.08	2.55	2.58	3.04	3.16
0.5	Present	1.29	1.36	2.04	2.15	2.72	3.01	3.44	3.87	4.21	4.69
	Ref [*a**]	1.30	1.37	2.05	2.15	2.73	3.01	3.45	3.88	4.22	4.71
1	Present	1.95	2.59	3.21	4.29	4.67	4.72	4.87	5.32	6.03	6.16
	Ref [*a**]	1.96	2.59	3.21	4.30	4.68	4.73	4.86	5.31	6.03	6.13
2	Present	2.77	4.69	5.21	5.21	5.57	6.90	7.84	8.08	8.61	8.84
3	Present	3.39	4.71	5.68	7.76	7.78	8.12	8.40	8.97	10.64	10.98

*a**: Shi et al. (2014)

Table 5 Non-dimensional frequency parameter $\Omega = \sqrt[4]{\omega^2 \rho h a^2 b^2 / D_{11}}$ for rectangular S–S–S–S orthotropic plates M1

a/*b*	Method	Mode sequence									
		1	2	3	4	5	6	7	8	9	10
0.33	Present	3.16	3.22	3.34	3.55	3.84	4.21	4.64	5.10	5.60	6.12
	Ref [*a**]	3.16	3.21	3.32	3.51	3.79	4.15	4.58	5.05	5.55	6.06
0.5	Present	3.18	3.34	3.68	4.21	4.86	5.60	6.30	6.37	6.38	6.49
	Ref [*a**]	3.18	3.32	3.64	4.15	4.81	5.55	6.30	6.33	6.35	6.45
1	Present	3.34	4.21	5.60	6.37	6.69	7.18	7.37	8.42	8.84	9.48
	Ref [*a**]	3.32	4.15	5.55	6.35	6.63	7.14	7.28	8.31	8.80	9.47
2	Present	4.21	6.69	7.18	8.42	9.66	10.52	10.64	11.20	12.62	12.73
3	Present	5.60	7.37	10.03	10.52	11.20	12.62	12.98	14.73	15.63	16.01

*a**: Shi et al. (2014)

4 Results and Discussion

The above analysis has been performed for a wide range of edge conditions of thin orthotropic rectangular plates, in order to demonstrate the versatility and stability of the proposed set of admissible functions. The accuracy and convergence of the present method have also been investigated and presented. The material properties of the thin

Table 6 Non-dimensional frequency parameter $\Omega = \sqrt[4]{\omega^2 \rho h a^2 b^2 / D_{11}}$ for rectangular C–S–C–F orthotropic plates M1

a/*b*	Method	Mode sequence									
		1	2	3	4	5	6	7	8	9	10
0.33	Present	4.73	4.74	4.76	4.81	4.91	5.06	5.26	5.53	5.85	6.23
	Ref [*a**]	4.73	4.87	5.39	6.43	7.83	7.86	7.94	8.17	8.67	9.39
0.5	Present	4.73	4.75	4.83	5.00	5.29	5.73	6.28	6.93	7.64	7.84
	Ref [*a**]	4.73	4.76	4.83	4.99	5.28	5.71	6.26	6.92	7.63	7.85
1	Present	4.73	4.88	5.41	6.45	7.84	7.85	7.94	8.20	8.71	9.38
	Ref [*a**]	4.74	4.87	5.39	6.43	7.83	7.86	7.94	8.17	8.67	9.39
2	Present	4.76	5.65	7.87	8.23	8.33	9.84	11.00	11.31	11.42	12.25
3	Present	4.80	7.16	7.90	9.17	11.03	11.83	11.85	12.74	14.16	14.35

*a**: Shi et al. (2014)

Table 7 Non-dimensional frequency parameter $\Omega = \sqrt[4]{\omega^2 \rho h a^2 b^2 / D_{11}}$ for rectangular C–F–F–F orthotropic plates M1

a/*b*	Method	Mode sequence									
		1	2	3	4	5	6	7	8	9	10
0.33	Present	1.89	1.91	1.99	2.17	2.49	2.90	3.39	3.90	4.44	4.74
	Ref [*a**]	1.87	1.9	1.98	2.17	2.49	2.91	3.39	3.91	4.45	4.69
0.5	Present	1.89	1.94	2.14	2.61	3.28	4.04	4.73	4.76	4.82	4.89
	Ref [*a**]	1.87	1.93	2.14	2.61	3.28	4.05	4.69	4.72	4.79	4.87
1	Present	1.89	2.07	2.99	4.46	4.73	4.84	5.19	5.96	6.13	7.11
	Ref [*a**]	1.87	2.06	2.99	4.47	4.69	4.79	5.14	5.90	6.13	7.05
2	Present	1.89	2.42	4.72	5.07	5.35	6.63	7.91	8.09	8.69	8.97
3	Present	1.89	2.76	4.72	5.42	7.80	7.98	8.32	8.69	10.39	11.07

*a**: Shi et al. (2014)

Table 8 Non-dimensional frequency parameter $\Omega = \sqrt[4]{\omega^2 \rho h a^2 b^2 / D_{11}}$ for rectangular C–C–C–C orthotropic plates M1

a/*b*	Method	Mode sequence									
		1	2	3	4	5	6	7	8	9	10
0.33	Present	4.74	4.75	4.82	4.92	5.08	5.30	5.59	5.94	6.34	6.77
0.5	Present	4.75	4.83	5.03	5.36	5.83	6.43	7.11	7.84	7.86	7.91
1	Present	4.89	5.55	6.73	7.92	8.20	8.20	8.79	9.72	9.80	10.92
	Ref [*a**]	4.88	5.52	6.70	7.92	8.16	8.17	8.73	9.63	9.76	10.82
2	Present	6.05	8.38	8.95	10.22	11.28	12.26	12.39	12.98	14.33	14.42
3	Present	8.17	9.56	11.94	13.09	13.70	14.73	14.97	16.88	17.71	18.20

*a**: Shi et al. (2014)

Table 9 Non-dimensional frequency parameter $\Omega = \sqrt[4]{\omega^2 \rho h a^2 b^2 / D_{11}}$ for rectangular C–C–C–G orthotropic plates M1

a/*b*	Mode sequence									
	1	2	3	4	5	6	7	8	9	10
0.33	4.73	4.74	4.78	4.85	4.96	5.13	5.37	5.67	6.03	6.44
0.5	4.73	4.77	4.88	5.10	5.47	5.97	6.59	7.28	7.85	7.87
1	4.75	5.02	5.82	7.08	7.86	7.99	8.35	8.58	9.02	10.01
2	4.89	6.71	7.92	8.78	9.75	10.88	11.04	11.53	12.87	13.07
3	5.29	8.07	9.33	10.53	11.12	12.61	14.23	14.32	14.88	15.22

orthotropic rectangular plate are specified in Table 1. Two types of material have been used.

First, the most challenging classical boundary condition for vibration analysis, i.e., a completely free square orthotropic plate (FFFF), is considered. The convergence behavior

Table 10 Non-dimensional frequency parameter $\Omega = \sqrt[4]{\omega^2 \rho h a^2 b^2 / D_{11}}$ for rectangular G–G–C–C orthotropic plates M1

a/*b*	Mode sequence									
	1	2	3	4	5	6	7	8	9	10
0.33	2.35	2.40	2.53	2.79	3.16	3.61	4.11	4.64	5.18	5.47
0.5	2.36	2.50	2.91	3.55	4.31	5.12	5.47	5.52	5.63	5.83
1	2.43	3.37	4.91	5.49	5.75	6.44	6.58	7.56	8.28	8.61
2	3.03	5.62	6.15	7.21	8.67	9.47	9.57	10.08	11.42	11.78
3	4.10	5.96	8.82	9.14	9.67	11.08	11.86	13.28	14.31	14.58

Table 11 Non-dimensional frequency parameter $\Omega = \sqrt[4]{\omega^2 \rho h a^2 b^2 / D_{11}}$ for rectangular C–C–C–G orthotropic plates M2

a/*b*	Method	Mode sequence									
		1	2	3	4	5	6	7	8	9	10
0.4	Present	4.71	4.74	4.79	4.89	5.05	5.27	5.56	5.92	6.33	6.79
	Exact [*b**]	4.73	4.75	4.80	4.89	5.04	5.26	5.55	5.91	6.32	6.78
0.66	Present	4.72	4.80	5.01	5.40	5.97	6.70	7.52	7.83	7.88	8.00
	Exact [*b**]	4.73	4.80	5.01	5.38	5.96	6.69	7.52	7.86	7.90	8.00
1	Present	4.74	4.96	5.58	6.59	7.83	7.83	7.97	8.28	8.82	9.20
	Exact [*b**]	4.74	4.95	5.57	6.59	7.84	7.86	7.98	8.27	8.79	9.22
1.5	Present	4.77	5.46	7.02	7.86	8.21	9.01	9.06	10.45	10.98	11.16
	Exact [*b**]	4.78	5.44	7.02	7.86	8.2	9.03	9.04	10.41	11.02	11.21
2.5	Present	4.97	7.31	7.95	9.21	10.78	11.04	11.83	11.85	13.69	14.15
	Exact [*b**]	4.95	7.31	7.96	9.18	10.83	11.07	11.81	11.83	13.63	14.19

*b**: Xing and Xu (2013)

Table 12 Non-dimensional frequency parameter $\Omega = \sqrt[4]{\omega^2 \rho h a^2 b^2 / D_{11}}$ for rectangular S–G–C–C orthotropic plates M2

a/*b*	Method	Mode sequence									
		1	2	3	4	5	6	7	8	9	10
0.4	Present	3.90	3.94	4.03	4.20	4.44	4.76	5.14	5.59	6.07	6.59
	Exact [*b**]	3.90	3.93	4.04	4.20	4.42	4.72	5.10	5.54	6.02	6.54
0.66	Present	3.91	4.05	4.38	4.93	5.66	6.49	7.02	7.09	7.25	7.40
	Exact [*b**]	3.93	4.05	4.36	4.89	5.61	6.44	7.07	7.13	7.26	7.34
1	Present	3.93	4.31	5.17	6.37	7.04	7.21	7.62	7.74	8.29	9.17
	Exact [*b**]	3.95	4.29	5.13	6.32	7.08	7.23	7.60	7.69	8.24	9.12
1.5	Present	4.00	5.02	6.86	7.07	7.53	8.59	8.98	10.17	10.17	10.46
	Exact [*b**]	4.01	4.98	6.81	7.11	7.52	8.52	8.93	10.08	10.23	10.48
2.5	Present	4.32	7.18	7.18	8.77	10.24	10.82	11.21	11.70	13.33	13.34
	Exact [*b**]	4.30	7.13	7.21	8.70	10.30	10.77	11.17	11.60	13.21	13.41

*b**: Xing and Xu (2013)

for first ten non-dimensional frequency parameters of the square FFFF plate is reported in Table 2 and verified with Shi et al. (2014). It is seen that the first 20 terms in the set of admissible functions (in either direction) are sufficient for the convergence.

The convergence study for the square CCCC isotropic and orthotropic plates is presented in Table 3 and Fig. 3a, b. For the isotropic plate (Fig. 3a), the first 13 terms of the proposed set of admissible functions give an error of less than 0.1% from the exact frequency parameter. The error reduces to less than 0.01% with 25 terms. For the orthotropic plate (Fig. 3b), this error is less than 0.1% with the first 28 terms of admissible functions and reduces to less than 0.01% with 38 terms. The convergence of the frequency parameter up to the second decimal place is achieved with only 20 terms.

The influence of the plate aspect ratio on the non-dimensional frequency parameters (having classical boundary conditions) are given in Tables 4, 5, 6, 7, 8, 9, and 10 for the orthotropic plate of material M1, and in Tables 11, 12, and 13 for the orthotropic plate of material M2. The calculated non-dimensional frequencies shown are for the first ten

Table 13 Non-dimensional frequency parameter $\Omega = \sqrt[4]{\omega^2 \rho h a^2 b^2 / D_{11}}$ for rectangular G–G–C–C orthotropic plates M2

a/*b*	Method	Mode sequence									
		1	2	3	4	5	6	7	8	9	10
0.4	Present	2.35	2.42	2.60	2.92	3.35	3.85	4.39	4.96	5.47	5.50
	Exact [*b**]	2.37	2.42	2.59	2.90	3.32	3.82	4.37	4.93	5.50	5.51
0.66	Present	2.36	2.63	3.26	4.11	5.05	5.46	5.55	5.76	6.03	6.12
	Exact [*b**]	2.38	2.62	3.23	4.08	5.03	5.50	5.58	5.77	6.01	6.11
1	Present	2.41	3.15	4.45	5.48	5.72	5.90	6.28	7.19	7.40	8.34
	Exact [*b**]	2.42	3.13	4.42	5.51	5.73	5.88	6.26	7.13	7.35	8.27
1.5	Present	2.58	4.27	5.54	6.18	6.47	7.59	8.64	8.73	8.99	9.47
	Exact [*b**]	2.56	4.24	5.55	6.12	6.43	7.52	8.67	8.69	8.97	9.38
2.5	Present	3.27	5.71	6.84	7.84	8.73	9.94	10.64	11.18	11.82	12.44
	Exact [*b**]	3.22	5.71	6.80	7.76	8.75	9.87	10.61	11.09	11.85	12.32

*b**: Xing and Xu (2013)

Table 14 Non-dimensional frequency parameter $\Omega = \sqrt[4]{\omega^2 \rho h a^2 b^2 / D_{11}}$ for orthotropic plates M1 versus K_R, with $K_T = 10^8$

K_R	*a*/*b* = 1			*a*/*b* = 0.8			*a*/*b* = 0.6			*a*/*b* = 0.4		
	Mode 1	Mode 2	Mode 3	Mode 1	Mode 2	Mode 3	Mode 1	Mode 2	Mode 3	Mode 1	Mode 2	Mode 3
0	3.343	4.208	5.598	3.260	3.775	4.725	3.203	3.455	3.979	3.167	3.260	3.455
1	3.668	4.584	5.946	3.542	4.081	5.010	3.465	3.717	4.220	3.423	3.509	3.687
10	4.366	5.158	6.449	4.261	4.695	5.520	4.201	4.389	4.792	4.170	4.229	4.355
20	4.562	5.303	6.555	4.468	4.866	5.649	4.413	4.584	4.956	4.385	4.438	4.553
30	4.651	5.369	6.602	4.561	4.944	5.708	4.508	4.672	5.032	4.481	4.532	4.643
50	4.735	5.432	6.647	4.648	5.019	5.764	4.597	4.755	5.103	4.572	4.621	4.727
5e2	4.872	5.537	6.721	4.790	5.141	5.859	4.743	4.892	5.222	4.718	4.765	4.866
10^3	4.880	5.543	6.726	4.799	5.149	5.865	4.752	4.900	5.230	4.727	4.774	4.874
10^4	4.888	5.550	6.730	4.807	5.156	5.870	4.760	4.908	5.237	4.736	4.782	4.882
10^5	4.889	5.550	6.731	4.808	5.157	5.871	4.761	4.909	5.238	4.736	4.783	4.883
5e5	4.889	5.550	6.731	4.808	5.157	5.871	4.761	4.909	5.238	4.737	4.783	4.883
10^6	4.889	5.550	6.731	4.808	5.157	5.871	4.761	4.909	5.238	4.737	4.783	4.883
5e6	4.889	5.550	6.731	4.808	5.157	5.871	4.761	4.909	5.238	4.737	4.783	4.883
10^8	4.889	5.550	6.731	4.808	5.157	5.871	4.761	4.909	5.238	4.737	4.783	4.883

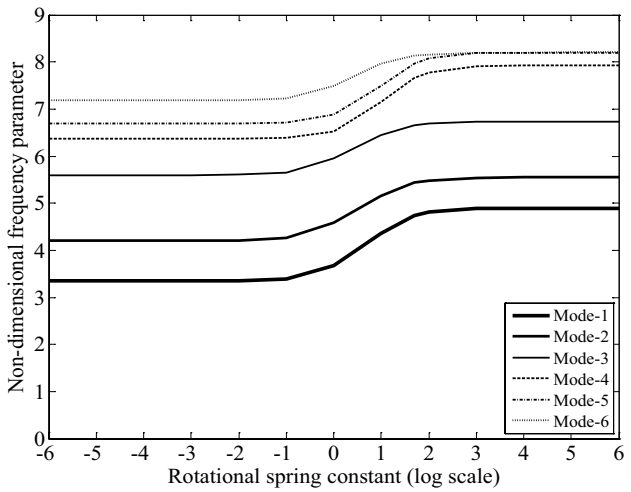

Fig. 4 Frequency parameter of orthotropic plate (M_1) with various values of rotational spring constant

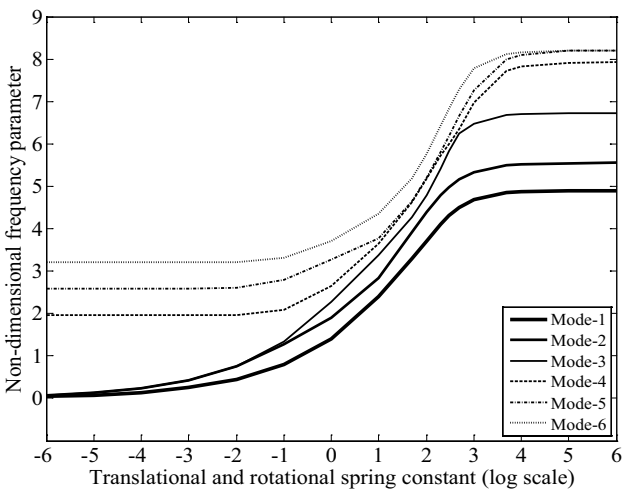

Fig. 5 Frequency parameter of orthotropic plate (M_1) with variable translational and rotational spring constant

Table 15 Non-dimensional frequency parameter $\Omega = \sqrt[2]{\omega^2 \rho h a^2 b^2 / D}$ for square isotropic plates $\left(D = Eh^3/12\left(1-\nu^2\right)\right)$

Case		Mode sequence									
		1	2	3	4	5	6	7	8	9	10
1	SSSS	19.739	49.351	49.351	78.960	98.716	98.716	128.321	128.321	167.841	167.841
2	SCSC	28.950	54.744	69.328	94.589	102.220	129.102	140.214	154.787	170.358	199.831
3	SCSS	23.639	51.677	58.621	86.130	100.294	113.204	133.820	140.853	169.025	187.436
4	SCSF	12.681	33.023	41.699	62.976	72.289	90.618	103.060	111.870	131.230	152.688
5	SSSF	11.682	27.736	41.198	59.042	61.808	90.316	94.424	108.911	115.588	145.587
6	SFSF	9.632	16.135	36.726	38.949	46.743	70.748	75.284	88.012	96.068	111.035
7	CCCC	35.993	73.424	73.424	108.288	131.689	132.307	165.183	165.183	210.744	210.744
8	CCCS	31.825	63.317	71.098	100.826	116.351	130.446	151.961	159.619	189.792	209.554
9	CCCF	23.928	39.976	63.251	76.635	80.583	116.642	122.341	134.288	140.344	172.797
10	CCSS	27.057	60.548	60.802	92.867	114.582	114.785	145.862	146.169	188.507	188.758
11	CCSF	17.547	35.994	51.863	71.088	74.237	105.919	109.324	125.468	132.638	164.147
12	CCFF	6.921	23.912	26.589	47.670	62.720	65.558	85.750	88.376	121.388	124.122
13	CSCF	23.378	35.566	62.904	66.729	77.391	108.868	118.958	122.099	137.880	159.719
14	CSSF	16.805	31.103	51.448	63.977	67.560	101.094	105.644	117.119	122.759	153.652
15	CSFF	5.357	19.070	24.710	43.114	52.671	63.881	77.497	83.768	106.235	120.486
16	CFCF	22.175	26.422	43.616	61.204	67.220	79.844	87.658	120.204	124.548	126.849
17	CFSF	15.209	20.597	39.745	49.504	56.334	77.334	78.582	103.562	110.856	117.308
18	CFFF	3.478	8.519	21.328	27.213	31.007	54.256	61.380	64.165	71.093	93.006
19	SSFF	3.367	17.317	19.294	38.213	51.039	53.492	72.973	74.638	104.732	107.258
20	SFFF	0.000	6.650	14.917	25.399	26.008	48.498	50.623	58.797	65.196	88.051
21	FFFF	0.000	0.000	0.000	13.469	19.596	24.270	34.803	34.803	61.094	61.094
22	SSSG	12.334	32.067	41.946	61.667	71.547	91.312	101.134	111.026	130.776	150.475
23	SCSG	13.680	38.666	42.586	66.274	83.440	91.723	110.965	114.357	147.820	158.390
24	SGSF	9.737	17.681	39.192	42.359	47.967	74.509	86.218	88.387	97.363	119.049
25	SGSG	9.870	19.739	39.482	49.348	49.351	78.958	88.849	98.695	98.716	128.305
26	CSCG	23.816	39.086	63.549	75.844	79.535	114.794	123.008	133.764	139.704	170.896
27	CSSG	17.343	35.049	52.144	69.934	73.436	106.598	107.424	124.725	132.129	162.044
28	SSGG	4.935	24.674	24.674	44.414	64.157	64.157	83.895	83.895	123.374	123.387
29	CSGG	7.243	25.557	32.301	49.976	64.660	76.901	87.802	94.885	123.736	132.257
30	SSGF	4.034	18.809	24.012	41.170	52.981	63.294	75.790	81.609	107.051	117.732
31	SCGF	5.700	24.695	24.908	45.737	63.687	64.304	85.023	85.336	122.516	123.374
32	SGGF	2.408	9.180	21.998	30.518	33.402	56.192	61.316	70.238	77.533	97.459
33	SFGF	2.378	6.887	21.822	26.379	29.222	51.676	61.007	65.223	69.003	90.841
34	CGSG	15.433	23.656	50.015	51.680	58.691	86.171	100.276	104.372	113.348	133.826
35	CGCG	22.375	28.955	54.751	61.689	69.348	94.620	102.231	120.981	129.185	140.261
36	SGGG	2.467	12.340	22.207	32.086	41.949	61.690	61.705	71.570	91.296	101.200
37	CGGG	5.600	13.692	30.254	38.728	42.592	66.340	74.712	83.569	91.709	111.108
38	SGFG	0.00	11.687	15.434	27.777	41.200	50.018	59.095	61.920	90.299	94.559
39	CGFG	3.523	12.694	22.077	33.109	41.708	61.819	63.065	72.522	90.619	103.300
40	GGFG	0.000	5.600	9.736	17.690	30.256	39.188	42.411	47.971	74.549	74.713
41	FGFG	0.000	0.000	9.631	16.135	22.373	36.726	38.945	46.740	61.673	70.746
42	GGGG	0.000	9.869	9.869	19.739	39.478	39.478	49.348	49.348	78.956	88.826
43	CCCG	24.577	44.751	63.998	83.278	87.218	123.327	123.688	142.456	150.517	181.903
44	CCSG	18.356	41.230	52.675	74.098	85.103	106.958	116.805	127.754	149.042	169.505
45	CCGF	7.779	25.818	32.247	51.200	64.821	76.417	89.237	95.884	123.730	134.376
46	CCGG	8.996	32.895	33.057	55.018	77.207	77.339	98.219	98.510	140.599	141.312
47	CGCF	22.264	27.501	48.524	61.423	68.227	90.242	90.845	120.549	127.999	131.814
48	CGSF	15.309	21.905	45.041	49.736	57.445	82.053	88.026	103.923	112.080	124.958

Table 15 (continued)

Case		Mode sequence									
		1	2	3	4	5	6	7	8	9	10
49	CSGF	6.608	19.946	31.708	47.055	53.591	76.083	80.076	92.788	107.453	126.951
50	CGGF	5.549	10.903	30.054	34.203	37.361	61.211	74.351	78.019	82.341	103.905
51	CFGF	5.515	8.998	27.370	29.889	36.220	57.030	65.799	74.054	81.193	94.875
52	SGFF	0.00	8.700	15.289	26.384	32.845	49.621	53.868	60.787	76.645	91.061
53	CGFF	3.500	10.186	21.882	31.460	34.022	58.112	61.539	71.256	77.304	99.651
54	GGFF	0.000	4.899	6.068	15.922	29.277	30.612	40.377	42.122	70.284	73.427
55	GFFF	0.000	0.000	5.372	14.625	22.004	29.708	36.052	40.076	61.269	66.853

Table 16 First six non-dimensional frequency parameters for a square isotropic plate with all edges rotationally restrained (RRRR)

K_R	Method	Mode sequence $\Omega = \sqrt[4]{\omega^2 \rho h a^2 b^2 / D}$					
		1	2	3	4	5	6
0.1	Present	19.936	49.547	49.547	79.155	98.899	98.900
	Ref [c^*]	19.936	49.546	49.546	79.155	98.895	98.895
1.00	Present	21.502	51.192	51.192	80.828	100.588	100.595
	Ref [c^*]	21.505	51.195	51.195	80.831	100.587	100.594
10.00	Present	28.502	60.219	60.219	90.819	111.202	111.424
	Ref [c^*]	28.583	60.337	60.337	90.957	111.352	111.578
20.00	Present	31.081	64.309	64.309	95.828	116.857	117.233
	Ref [c^*]	31.219	64.342	64.535	96.112	117.181	117.566
100	Present	34.672	70.785	70.785	104.466	127.044	127.627
	Ref [c^*]	34.918	71.259	71.259	105.128	127.848	128.439
1000.00	Present	35.843	73.109	73.109	107.805	131.085	131.704
	Ref [c^*]	36.134	73.694	73.694	108.658	132.129	132.756

c^*: Zhang et al. (2019)

Table 17 Fundamental frequency parameter $\Omega = \sqrt{\omega^2 \rho h a^2 b^2 / D_{11}}$ for the rectangular orthotropic plates with three edges simply supported and one edge rotationally restrained (SRRR) with $D_{11}/H = D_{11}/H = 0.5$, $H = D_{12} + 2D_{66}$

K_R	$b/a = 0.5$			$b/a = 1.0$			$b/a = 1.5$		
	Ref [c^*]	Present	(%)	Ref [c^*]	Present	(%)	Ref [c^*]	Present	(%)
0.000	56.697	56.695	−0.002	24.176	24.175	−0.003	16.971	17.024	0.313
1.000	59.130	59.130	0.000	24.545	24.546	0.007	17.096	17.131	0.203
10.000	68.068	67.957	−0.163	26.153	26.140	−0.053	17.725	17.654	−0.402
∞	75.781	75.441	−0.450	27.969	27.891	−0.281	18.542	18.384	−0.858

c^*: Zhang et al. (2019)

modes of free vibration with five different aspect ratios and verified with the literature.

All the above results presented in Tables 4, 5,6, 7, 8, 9, 10, 11, 12, and 13 have been limited to plates with classical boundary conditions, which are the extreme cases of the non-classical elastically constrained edges.

This study is further extended to the free vibration analysis of non-classical boundary conditions, using a wide range of spring constants K_T, K_R for modeling the edge support. First, we consider a simply supported thin rectangular plate for various rotational stiffness parameters K_R. Table 14 shows the frequency parameters of the orthotropic SSSS plate with varying elastic rotational spring stiffness, for four different aspect ratios of 1, 0.8, 0.6, and 0.4. It is seen that non-dimensional frequency parameters are significantly affected by the edge conditions and the plate aspect ratio. A lower edge spring constant leads to a lower frequency (approaching an SSSS plate), while making the edge stiffer increases the natural frequency (approaching a CCCC plate). This is consistently seen for

Table 18 Non-dimensional translational and rotational spring constants for various edge conditions of plate

Boundary conditions		Side-1		Side-2		Side-3		Side-4	
		K_T	K_R	K_T	K_R	K_T	K_R	K_T	K_R
1	SSSS	10^8	0	10^8	0	10^8	0	10^8	0
2	SCSC	10^8	0	10^8	10^8	10^8	0	10^8	10^8
3	SCSS	10^8	0	10^8	10^8	10^8	0	10^8	0
4	SCSF	10^8	0	10^8	10^8	10^8	0	0	0
5	SSSF	10^8	0	10^8	0	10^8	0	0	0
6	SFSF	10^8	0	0	0	10^8	0	0	0
7	CCCC	10^8	10^8	10^8	10^8	10^8	10^8	10^8	10^8
8	CCCS	10^8	10^8	10^8	10^8	10^8	10^8	10^8	0
9	CCCF	10^8	10^8	10^8	10^8	10^8	10^8	0	0
10	CCSS	10^8	10^8	10^8	10^8	10^8	0	10^8	0
11	CCSF	10^8	10^8	10^8	10^8	10^8	0	0	0
12	CCFF	10^8	10^8	10^8	10^8	0	0	0	0
13	CSCF	10^8	10^8	10^8	0	10^8	10^8	0	0
14	CSSF	10^8	10^8	10^8	0	10^8	0	0	0
15	CSFF	10^8	10^8	10^8	0	0	0	0	0
16	CFCF	10^8	10^8	0	0	10^8	10^8	0	0
17	CFSF	10^8	10^8	0	0	10^8	0	0	0
18	CFFF	10^8	10^8	0	0	0	0	0	0
19	SSFF	10^8	0	10^8	0	0	0	0	0
20	SFFF	10^8	0	0	0	0	0	0	0
21	FFFF	0	0	0	0	0	0	0	0
22	SSSG	10^8	0	10^8	0	10^8	0	0	10^8
23	SCSG	10^8	0	10^8	10^8	10^8	0	0	10^8
24	SGSF	10^8	0	0	10^8	10^8	0	0	0
25	SGSG	10^8	0	0	10^8	10^8	0	0	10^8
26	CSCG	10^8	10^8	10^8	0	10^8	10^8	0	10^8
27	CSSG	10^8	10^8	10^8	0	10^8	0	0	10^8
28	SSGG	10^8	0	10^8	0	0	10^8	0	10^8
29	CSGG	10^8	10^8	10^8	0	0	10^8	0	10^8
30	SSGF	10^8	0	10^8	0	0	10^8	0	0
31	SCGF	10^8	0	10^8	10^8	0	10^8	0	0
32	SGGF	10^8	0	0	10^8	0	10^8	0	0
33	SFGF	10^8	0	0	0	0	10^8	0	0
34	CGSG	10^8	10^8	0	10^8	10^8	0	0	10^8
35	CGCG	10^8	10^8	0	10^8	10^8	10^8	0	10^8
36	SGGG	10^8	0	0	10^8	0	10^8	0	10^8
37	CGGG	10^8	10^8	0	10^8	0	10^8	0	10^8
38	SGFG	10^8	0	0	10^8	0	0	0	10^8
39	CGFG	10^8	10^8	0	10^8	0	0	0	10^8
40	GGFG	0	10^8	0	10^8	0	0	0	10^8
41	FGFG	0	0	0	10^8	0	0	0	10^8
42	GGGG	0	10^8	0	10^8	0	10^8	0	10^8
43	CCCG	10^8	10^8	10^8	10^8	10^8	10^8	0	10^8
44	CCSG	10^8	10^8	10^8	10^8	10^8	0	0	10^8
45	CCGF	10^8	10^8	10^8	10^8	0	10^8	0	0
46	CCGG	10^8	10^8	10^8	10^8	0	10^8	0	10^8
47	CGCF	10^8	10^8	0	10^8	10^8	10^8	0	0

Table 18 (continued)

Boundary conditions		Side-1		Side-2		Side-3		Side-4	
		K_T	K_R	K_T	K_R	K_T	K_R	K_T	K_R
48	CGSF	10^8	10^8	0	10^8	10^8	0	0	0
49	CSGF	10^8	10^8	10^8	0	0	10^8	0	0
50	CGGF	10^8	10^8	0	10^8	0	10^8	0	0
51	CFGF	10^8	10^8	0	0	0	10^8	0	0
52	SGFF	10^8	0	0	10^8	0	0	0	0
53	CGFF	10^8	10^8	0	10^8	0	0	0	0
54	GGFF	0	10^8	0	10^8	0	0	0	0
55	GFFF	0	10^8	0	0	0	0	0	0

all aspect ratios and all modes of vibration. A squarish plate (aspect ratio ~ 1) has a higher frequency than a more rectangular plate. This is because the beam mode shapes from the longer side dominate the vibration, neglecting the same from the shorter side. There is less density of nodal lines, leading to lower strain potential energy.

Figure 4 shows that the frequency parameters $\Omega = \sqrt[4]{\omega^2 \rho h a^2 b^2 / D_{11}}$ are functions of the rotational spring constant. Square orthotropic plate edges are modeled with a very large translational spring constant $K_T = 10^8$ and varying rotational spring constant K_R. It is observed that with an increase in rotational spring constant, the non-dimensional frequency parameters also increase. When rotational spring constant (K_R) is ~ 10^{-6}, the plate appears to vibrate as a simply supported (SSSS) plate. When $K_R \sim 10^6$, the plate behaves like a fully clamped (CCCC) plate. Therefore, the fundamental natural frequency of the SSSS plate is observed to deviate to the fundamental frequency of CCCC plate with the increase in rotational spring constant K_R. The conspicuous transition of SSSS plate behavior to CCCC plate behavior occurs at $10^1 < K_R < 10^3$. The transition region separates the ranges of edged spring constants where the non-classical plate can be assumed to behave like for practical engineering analysis. It helps in taking a time-bound engineering decision without having to resort to the complicated non-classical analysis (which may not be possible in several commercial CAD tools).

Figure 5 shows the frequency parameters $\Omega = \sqrt[4]{\omega^2 \rho h a^2 b^2 / D_{11}}$ of a square orthotropic plate with the edges constrained with rotational and translational spring stiffness. It is noticed that when both stiffnesses are very small in magnitude (10^{-6} order), the plate vibrates like a completely free plate (FFFF) and exhibits three rigid-body modes. When both the stiffnesses increase, the trivial frequency parameters of FFFF plate bifurcate to the frequency characteristics of the CCCC plate. The conspicuous transition of FFFF plate behavior to the CCCC plate behavior occurs at $10^{-3} < K_T, K_R < 10^3$.

The present method is capable of analyzing the free vibration of orthotropic and isotropic plates for a wide range of non-classical boundary conditions. In order to demonstrate this approach for isotropic plates, all the 55 possible classical boundary conditions [the combination of clamped (C), free (F), sliding (G), and simply supported (S)] have been analyzed by the Rayleigh–Ritz method with the proposed set of admissible functions. The first ten non-dimensional frequency parameters are shown in Table 15. The results show that in most cases, the non-dimensional frequency parameters of isotropic plates converge to the exact results (where these are available) to at least four significant numbers for any geometric edge condition. This establishes the efficacy of the present set of trial functions.

The non-dimensional frequency parameters for a square isotropic plate have rotationally restrained edges. The effect of the K_R is investigated for the first six modes and compared with those by Zhang et al. (2019), as mentioned in Table 16. Next, the rectangular orthotropic plates with three edges simply supported and one edge restrained with rotational spring of variable stiffness are investigated. The effect of the aspect ratio and rotational spring constant on the non-dimensional fundamental frequency parameter is tabulated in Table 17 and compared with the results of Zhang et al. (2019). Finally, the magnitudes of spring constants (for both translational and rotational springs) used for modeling various classical boundary conditions of the plate are summarized in Table 18.

5 Conclusion

A new complete set of admissible functions has been proposed to be incorporated in the energy-based Rayleigh–Ritz method for determining the frequency parameters of rectangular plates for arbitrary (non-classical) boundary conditions. The non-classical edge conditions are modeled as translational and rotational spring stiffness on the edges. The complete set of admissible functions (consisting of unit

function, linear function, the lowest order polynomial, and trigonometric functions) shows an excellent convergence capability for various boundary conditions, aspect ratios, and modes of vibration, without ill-conditioning. This efficacy is seen for both isotropic and orthotropic plates. The accuracy and convergence of the present method are shown through examples of various boundary conditions with both isotropic and orthotropic materials. The non-dimensional frequency parameters have been shown to converge to the exact value up to the third decimal place for most of the boundary conditions. The effects of elastic support stiffness and plate aspect ratio on the frequency parameters have also been studied. The present work establishes an efficient method for selecting a set of admissible functions that can be invariably implemented to plate with any classical and non-classical boundary conditions. This work provides an easy and quick technique to obtain a wide range of frequency parameters for both isotropic and orthotropic rectangular plates.

References

Ahmadian MT, Zangeneh MS (2002) Vibration analysis of orthotropic rectangular plates using superelements. Comput Methods Appl Mech Eng 191(19–20):2097–2103

Bapat AV, Venkatramani N, Suryanarayan S (1988) Simulation of classical edge conditions by finite elastic restraints in the vibration analysis of plates. J Sound Vib 120(1):127–140

Biancolini ME, Brutti C, Reccia L (2005) Approximate solution for free vibrations of thin orthotropic rectangular plates. J Sound Vib 288(1–2):321–344

Dalaei M, Kerr AD (1996) Natural vibration analysis of clamped rectangular orthotropic plates. J Sound Vib 189(3):399–406

Datta N, Verma Y (2018) Analytical scrutiny and prominence of beamwise rigid-body modes in vibration of plates with translational edge restraints. Int J Mech Sci 135:124–132

Dickinson SM, Di Blasio A (1986) On the use of orthogonal polynomials in the Rayleigh–Ritz method for the study of the flexural vibration and buckling of isotropic and orthotropic rectangular plates. J Sound Vib 108:51–62

Gorman DJ (1982) Free vibration analysis of rectangular plates. Elsevier, New York

Gorman DJ (1990) Accurate free vibration analysis of clamped orthotropic plates by the method of superposition. J Sound Vib 140(3):391–411

Gorman DJ (1993) Accurate free vibration analysis of the completely free orthotropic rectangular plate by the method of superposition. J Sound Vib 165(3):409–420

Gorman DJ (1994) Free-vibration analysis of point-supported orthotropic plates. J Eng Mech 120(1):58–74

Hearmon RFS (1959) The frequency of flexural vibration of rectangular orthotropic plates with clamped or supported edges. J Appl Mech 26:537–540

Hsu M-H (2010) Vibration analysis of orthotropic rectangular plates on elastic foundations. Compos Struct 92(4):844–852

Huang M et al (2005) Free vibration analysis of orthotropic rectangular plates with variable thickness and general boundary conditions. J Sound Vib 288(4–5):931–955

Hurlebaus S, Gaul L, Wang J-S (2001) An exact series solution for calculating the eigenfrequencies of orthotropic plates with completely free boundary. J Sound Vib 244(5):747–759

Jafari AA, Eftekhari SA (2011) An efficient mixed methodology for free vibration and buckling analysis of orthotropic rectangular plates. Appl Math Comput 218(6):2670–2692

Li WL (2004) Vibration analysis of rectangular plates with general elastic boundary supports. J Sound Vib 273(3):619–635

Li J-J, Cheng C-J (2005) Differential quadrature method for nonlinear vibration of orthotropic plates with finite deformation and transverse shear effect. J Sound Vib 281(1–2):295–309

Meirovitch L (1975) Elements of vibration analysis. McGraw-Hill Science, Engineering & Mathematics, New York

Monterrubio LE, Ilanko S (2015) Proof of convergence for a set of admissible functions for the Rayleigh–Ritz analysis of beams and plates and shells of rectangular planform. Comput Struct 147:236–243

Oosterhout GM, Van Der Hoogt PJM, Spiering R (1995) Accurate calculation methods for natural frequencies of plates with special attention to the higher modes. J Sound Vib 183(1):33–47

Rossi RE, Bambill DV, Laura PAA (1998) Vibrations of a rectangular orthotropic plate with a free edge: a comparison of analytical and numerical results. Ocean Eng 25(7):521–527

Shi D et al (2014) Free transverse vibrations of orthotropic thin rectangular plates with arbitrary elastic edge supports. J VibroEng 16(1):389–398

Verma Y, Datta N (2018) Application of translational edge restraint for vibration analysis of free edge Kirchhoff's plate including rigid-body modes. Eng Trans 66(1):21–60

Xing YF, Liu B (2009) New exact solutions for free vibrations of thin orthotropic rectangular plates. Compos Struct 89(4):567–574

Xing YF, Xu TF (2013) Solution methods of exact solutions for free vibration of rectangular orthotropic thin plates with classical boundary conditions. Compos Struct 104:187–195

Zhang S, Xu L, Li R (2019) New exact series solutions for transverse vibration of rotationally-restrained orthotropic plates. Appl Math Model 65:348–360